The Effect of Surface Microinjury on the Behavior of Aortic Valve Calcification

Yage LIU [1], Jingjing ZHANG [1], Wahab ABDUL [1], Chengyao NI [2], Ruibo ZHAO [1], Xiangdong KONG [1] *

[1] *School of Materials Science & Engineering, Zhejiang Sci-Tech University, Hangzhou 310018, China*
[2] *Zhejiang University, Affiliated Hospital 1, Hangzhou 310003, China*

http://doi.org/10.5755/j02.ms.37636

Received 17 June 2024; accepted 4 July 2024

Calcific Aortic Valve Disease (CAVD) is a disease in which a patient's aortic valve is biomineralized to form calcified plaques and cause damage to valve function, thus affecting the normal flow of blood to the heart. CAVD can lead to stenosis or insufficient closure of heart valves, which may lead to serious complications such as abnormal blood flow to the heart. The main components of natural valves are collagen, elastin, and glycosaminoglycans, of which collagen can be used as a nucleation site for calcium deposition, and when the valve surface suffers microinjury, the exposed collagen can easily induce calcium deposition and lead to the disease. In this study, we constructed a porcine aortic valve surface damage model to simulate the calcification process of the aortic valve *in vitro*. We analyzed the relevant samples by Scanning Electron Microscopy (SEM), Energy Spectrum Analysis (EDS), X-ray Powder Diffraction (XRD), Fourier Transform Infrared Spectroscopy Attenuation Total Reflection (FTIR-ATR), and Thermo-Gravimetric Analysis (TGA). The SEM and EDS spectroscopy confirmed that calcium deposition at the damaged parts of the valves was faster and that the sample contained a high concentration of calcium.; XRD analysis showed that the composition of the deposits was mainly dicalcium phosphate dihydrate (DCPD) and hydroxyapatite (HAp); FTIR-ATR results showed that the calcium deposits were carbonate-containing phosphates; TGA results further demonstrated that microinjury of heart valves accelerated the process of calcification and facilitated calcium deposition. The *in vitro* surface microinjury model used in this study is expected to be an effective model for rapid simulation of the *in vivo* calcification process.
Keywords: aortic valve, collagen, surface morphology, microinjury, calcification, biomineralization.

1. INTRODUCTION

Calcific Aortic Valve Disease (CAVD) is a common heart valve disease, with clinical manifestations of valve fibrosis and calcification, resulting in impaired leaflet motion, insufficient closure, regurgitation, and other symptoms due to impaired valve function. The clinical manifestations of patients are chest pain, dyspnea, fatigue, and other phenomena, that seriously affect daily life and work. There are no effective drugs to cure CAVD, and some drugs can only delay the disease progression of CAVD [1]. Surgery and transcatheter aortic valve replacement are currently the most effective clinical treatment options. However, there are also post-treatment aortic regurgitation, acute kidney injury, and coronary artery occlusion [2, 3].

CAVD is also a degenerative disease that progresses with age, the patient's valve gradually develops degenerative connective tissue disease, followed by tissue fibrosis, leaflet thickening, and valve calcification. With increasing research, investigators have reported that CAVD is influenced by genetic factors, signaling pathways [4, 5], aging, estrogen, and hormone levels [6, 7], the systemic environment in vivo [8, 9], shear stress, and hemodynamic factors [10], resulting in a variety of factors including endothelial dysfunction/damage, lipid accumulation, aseptic inflammation, and overproduction, degradation, and redeposition of valve extracellular matrix, which ultimately leads to irreversible calcification of the leaflets. Normal aortic valves have a three-layered structure of fibrous, spongy, and ventricular layers [11], where the fibrous layer consists of collagen fibers, valvular interstitial cells, fibroblasts, dendritic cells, and immune cells (macrophages and leukocytes) [12, 13]; and the ventricular layer, oriented towards the left ventricle, consists of elastin fibers, fibroblasts, and smooth muscle cells [14, 15]. Some autonomic nerves and lymphatic vessels are usually present in the ventricular layer; the spongy layer is located between the fibrous and ventricular layers, and the spongy layer is enriched in glycosaminoglycans and contains only fewer cells [16 – 19]. Valve mineralization occurs in two ways: firstly, biomineralization induced by osteoblasts differentiated from valvular interstitial cells, a process similar to bone growth in which osteoblasts secrete collagen, proteoglycans, glycoproteins and non-collagenous proteins to bind calcium ions and regulate the formation and growth of HAp crystals through biomineralization; and secondly, dystrophic calcification, which is characterized by the persistent and slow deposition of apatite and the damaged fibers, low-density lipoproteins and apoptotic vesicles acting as nucleating structures. It may result from the transition from amorphous to crystalline calcium and phosphate in the blood [20, 21].

Biologically induced or controlled biomineralization is one of the prevalent phenomena in biological systems, and valvular calcification belongs to a type of biomineralization, and a large number of experimental studies have shown that

* Corresponding author. Tel.: +86-13858077558.
E-mail: *kongxd@zstu.edu.cn* (X. Kong)

collagen fibers induce controlled mineralization [22, 23]. Xue et al. [24] used a molecular dynamics simulation method to study the nucleation of HAp on the surface of collagen, in which it was found that clusters containing calcium and phosphate ions with different sizes and morphologies on the solution and collagen surfaces, especially near the glutamic acid-arginine, where the clusters were much larger than those at other locations. This heterogeneous distribution mentioned above suggests that the clusters containing calcium and phosphate ions are induced and controlled by the surface properties of the protein. Qin et al. [25] used molecular dynamics and metadynamics simulations to explore the adsorption of calcium and phosphate ions by the groove topography. By constructing the nanogroove model against the planar model respectively, it was found that the ion adsorption rate and probability at the grooves were higher than those at the planar surface. In addition, the cluster growth process on the groove surface was divided into two steps, the first step was the adsorption of negatively charged calcium-deficient HAp, and the second step was the adsorption of positively charged calcium-rich HAp. The grooves contribute to the uneven charge distribution of calcium phosphate (CaP) clusters, which accelerates ion precipitation, enhances the interaction between the grooves and CaP clusters, and accelerates the deposition of CaP clusters on the groove surface.

This study investigated the potential role of microinjuries in promoting calcification of heart valves. We hypothesized that tiny injuries on the valve surface could expose collagen fibers, a key structural component. These exposed fibers might then act as nucleation sites, attracting calcium and phosphorus from the bloodstream and initiating the mineralization process. Additionally, the grooves created by the microinjuries could further facilitate the deposition of these minerals, accelerating calcification [26]. To test this hypothesis, we employed an in vitro model. Microneedles were used to simulate microinjuries on pig aortic valves, which were then placed in a solution mimicking blood composition (SBF). This allowed us to systematically analyze the impact of microinjuries on valve calcification.

2. EXPERIMENTAL

The porcine aortic valves were dissected from fresh hearts (Xiaoshan Hongken Meat Processing Company Ltd), which were rinsed repeatedly with phosphate-buffered saline and processed for microinjury using microneedles. After a 24-hour fixation in 2.5 % glutaraldehyde, the valves were secured in silicone elastomers to ensure full surface contact with the SBF solution and prevent wobbling. The valves were then incubated in a 37 °C water bath for 3 – 5 days. After removal, the valves underwent dehydration and drying using a graded ethanol series (10 % to 100 %). Finally, the prepared samples were preserved for further testing. Details of the entire modeling and experimental procedure are illustrated in Fig. 1. The morphology and dimensions of the microneedles (NSZ-608T, Nanjing, China) were observed and measured using a stereomicroscope. This ensured control over the penetration depth during the valve injury simulation. After dehydration and drying using a graded alcohol series, valve at plane and injury surface morphology was examined with a field emission SEM (S-4800, Hitachi, Japan). Additionally, the EDS component of the electron microscope was used to analyze the elemental composition of the microneedles. XRD patterns were obtained using a D/Max 2200-PC diffractometer (Rigaku Corporation, Tokyo, Japan) equipped with Cu Kα radiation and a graphite monochromator. The measurements were conducted at room temperature, scanning a 2θ range of 10° to 60°. Dry valve samples were analyzed using FTIR-ATR on a Fourier Transform Infrared Spectrometer (Nicolet™ iS50, China) with a wavelength range of 2000 – 500 cm-1. Background subtraction and baseline correction were performed before each sample measurement. Finally, small pieces of the valve samples were placed in a crucible and analyzed using a TGA (TGA209F1, Netzsch, Germany). The instrument was set to operate in an air environment with a flow rate of 40 mL/min, a temperature range of 25 – 900 °C, and a heating rate of 10 °C/min.

3. RESULTS AND DISCUSSION

A microneedle with the dimensions shown in Fig. 2 a (diameter: 0.162 mm, insertion depth: 0.5 mm) was used to create controlled microinjuries on the valve surface.

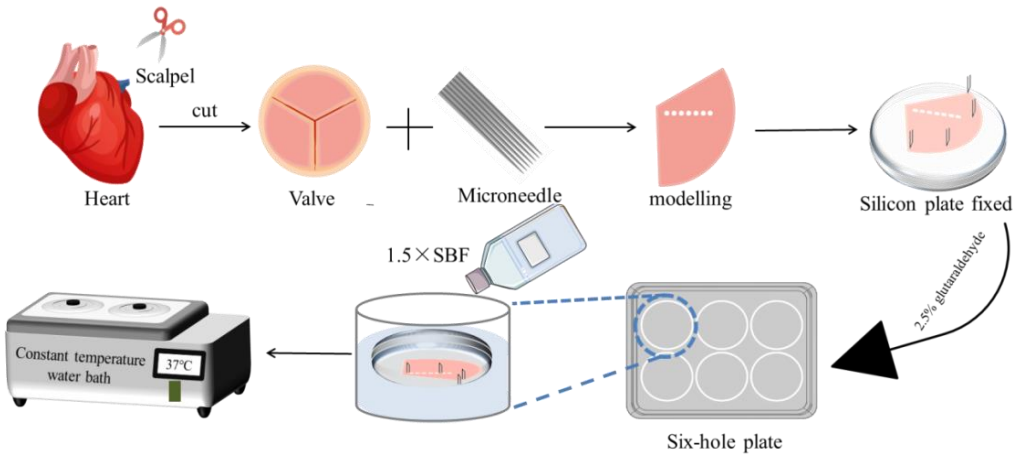

Fig. 1. Construction of aortic valve microinjury model and schematic diagram of the experimental procedure

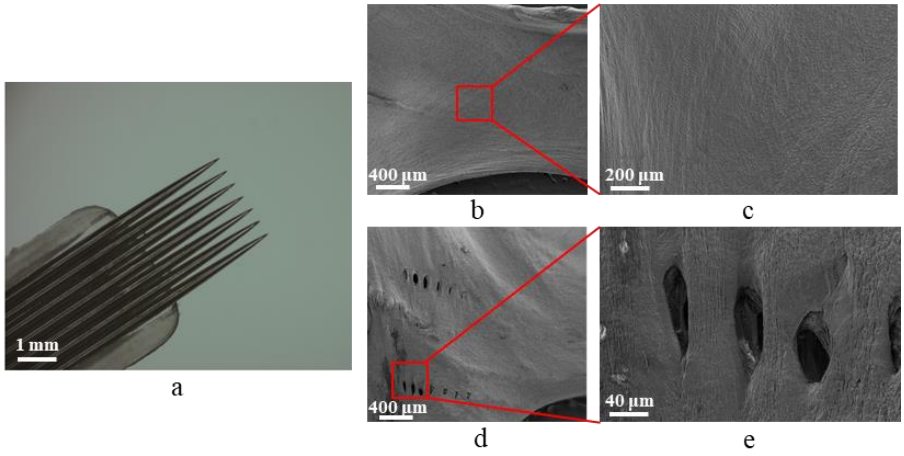

Fig. 2. a – microneedle images; b, c – SEM images of the valve surface before microneedle handling; d, e – after microneedle handling

As seen in Fig. 2 b and c, the untreated valve surface appeared smooth and flat. Following microneedle application (Fig. 2 d), the valve surface exhibited well-defined elliptical holes with deformed fibrous tissue visible between them. Due to the inherent elasticity and toughness of the valve tissue, dehydration, and drying using graded ethanol resulted in some pore deformation (Fig. 2 e). Nevertheless, this process successfully established a mechanical microinjury model on the valve surface. This model was then employed for immersion in simulated body fluids to investigate the impact of exposed valve tissue structure on calcification behavior.

Further analysis was performed using SEM to examine the valve surface morphology after immersion in the simulated body fluid. Fig. 3 a shows the valve surface after 3 days. Higher magnification images (Fig. 3 b) revealed the presence of particulate matter aggregates on the surface fibers. Notably, the undamaged valve flap surface remained smooth, with minimal deposits visible at this magnification (Fig. 3 c). Further magnification (Fig. 3 d) showed the growth and aggregation of submicron-sized, grape-like particles along the exposed fibers near the pores. A smaller number of scattered particles were also observed on the surface (Fig. 3 e). EDS analysis (Fig. 3 f and g) indicated a higher concentration of calcite near the holes compared to the flat surfaces of the valve.

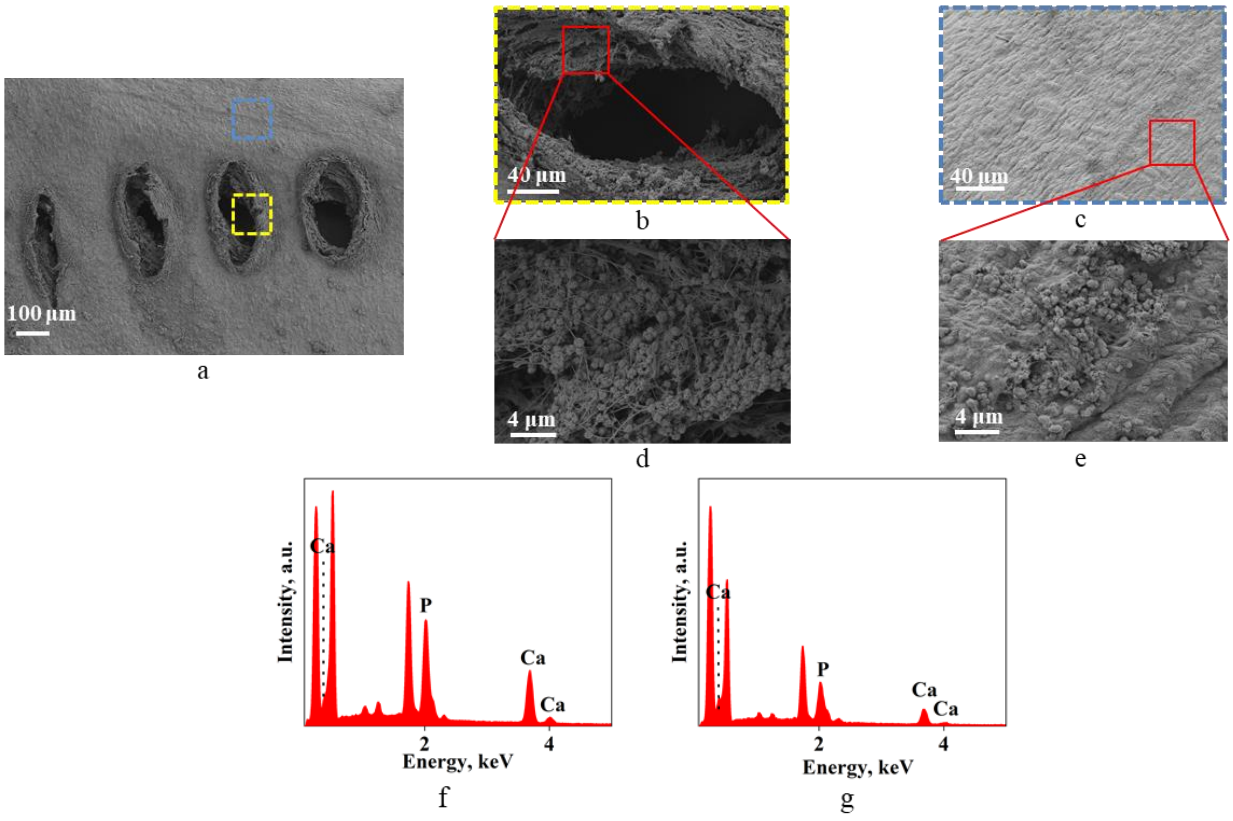

Fig. 3. SEM images and EDS energy spectra of valves in SBF with 3 days of calcification: a – overall surface morphology; b, c, d, e – enlarged image of the corresponding area; f, g – corresponding EDS energy spectrum

The surface morphology of the flap after 4 days of immersion is shown in Fig. 4 a. Compared to the 3-day sample, the overall surface appears rougher, with deposits visible at both the holes and flat areas. Higher magnification (Fig. 4 b) reveals elongated, strip-like deposits accumulating and growing around the valve opening, likely due to increased granular deposition. Smaller, nodular deposits are also evident on the surface (Fig. 4 c). With further immersion (Fig. 4 d and e), the fibrous tissue becomes obscured by a complete layer of sediment. Notably, the general morphology of the surface deposits remained similar. However, EDS analysis (Fig. 4 f and g) confirms a higher concentration of calcium near the holes compared to the flat regions of the valve.

The surface morphology of the flap after 5 days of immersion is shown in Fig. 5 a. As seen in Fig. 5 b, elongated, dense deposits accumulate near the valve openings. In contrast, deposits on the flat surfaces appear shorter and more dispersed (Fig. 5 c). Higher magnification (Fig. 5 d and e) reveals interconnected, spherical granular deposits growing along the valve surface. EDS analysis (Fig. 5 f and g) confirms the continuing trend of higher calcium concentration near the holes compared to the flat regions of the valve.

Analysis of the SEM images (Fig. 3, Fig. 4, and Fig. 5) and corresponding EDS data consistently revealed higher calcium deposition around the microinjury pores compared to the flat valve surfaces. This suggests that under identical immersion conditions, the microneedle-injured valve areas exhibited a greater tendency to capture calcium from the SBF solution. This enhanced capture likely facilitates calcium nucleation and subsequent growth near the pores, potentially due to exposed fibers and altered surface morphology.

XRD analyses of the flaps immersed for 3 – 5 days were performed separately to determine the physical phase composition of the calcium deposits on the flap surface. As shown in Fig. 6, the main positions of the diffraction peaks of the three groups of samples were at 21.3°, 23.7°, and 26.6°, respectively, and the half-peak widths were smaller, which indicated that the deposits were more crystalline. Overall, the main phase at 3 and 4 days of immersion was DCPD, with diffraction peaks at 21.3° (121) and 23.7° (040), but it also contained a small amount of HAp, with a diffraction peak at 26.6° (002). As soaking time increased, the HAp diffraction peaks became sharper in the XRD spectra of the valves soaked for 5 days. It indicates that apatite in the DCPD phase first forms on the valve surface when the valve is immersed in simulated body fluids, followed by a continuous conversion to the HAp phase. Most of the crystalline phases of cardiovascular deposits detected *in vivo* are more stable HAp [27], which may be due to the gradual transformation between the different crystalline phases of apatite and the eventual formation of stable HAp.

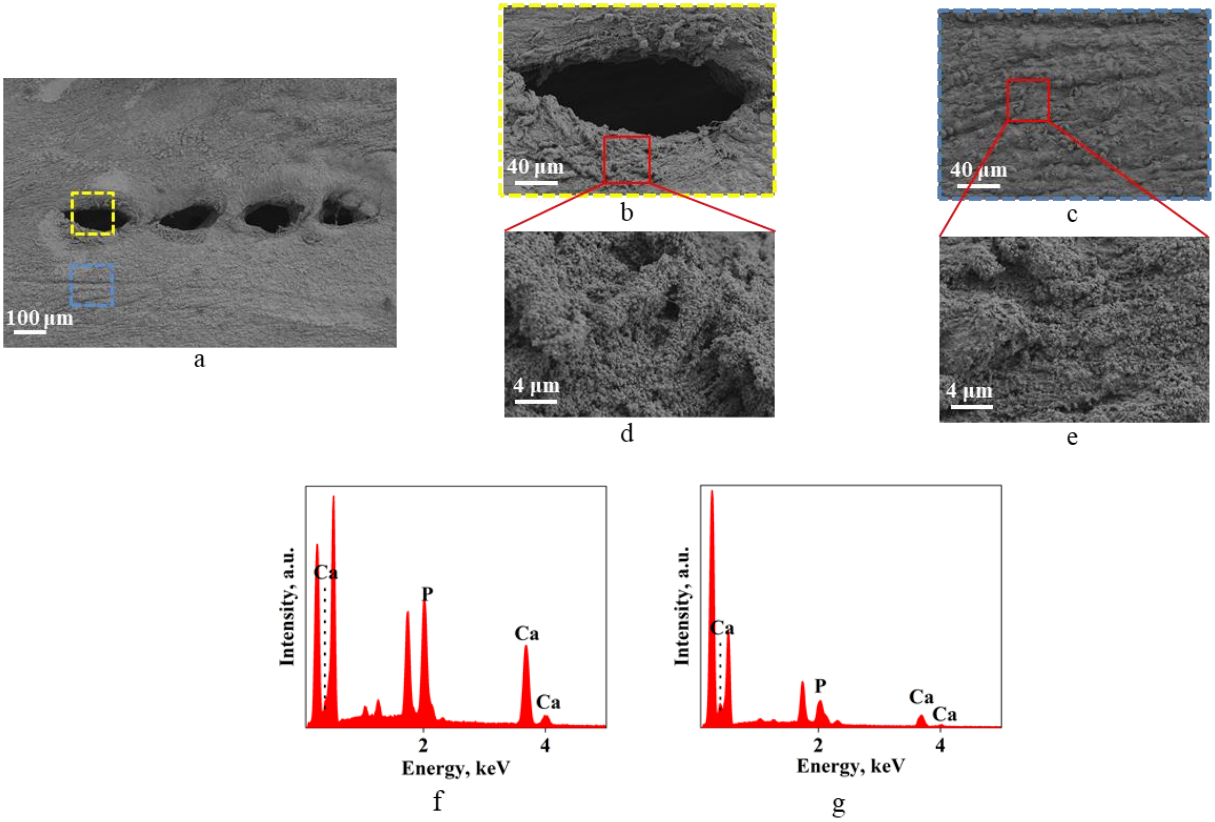

Fig. 4. SEM images and EDS energy spectra of valves in SBF with 4 days of calcification: a – overall surface morphology; b, c, d, e – enlarged image of the corresponding area; f, g – corresponding EDS energy spectrum

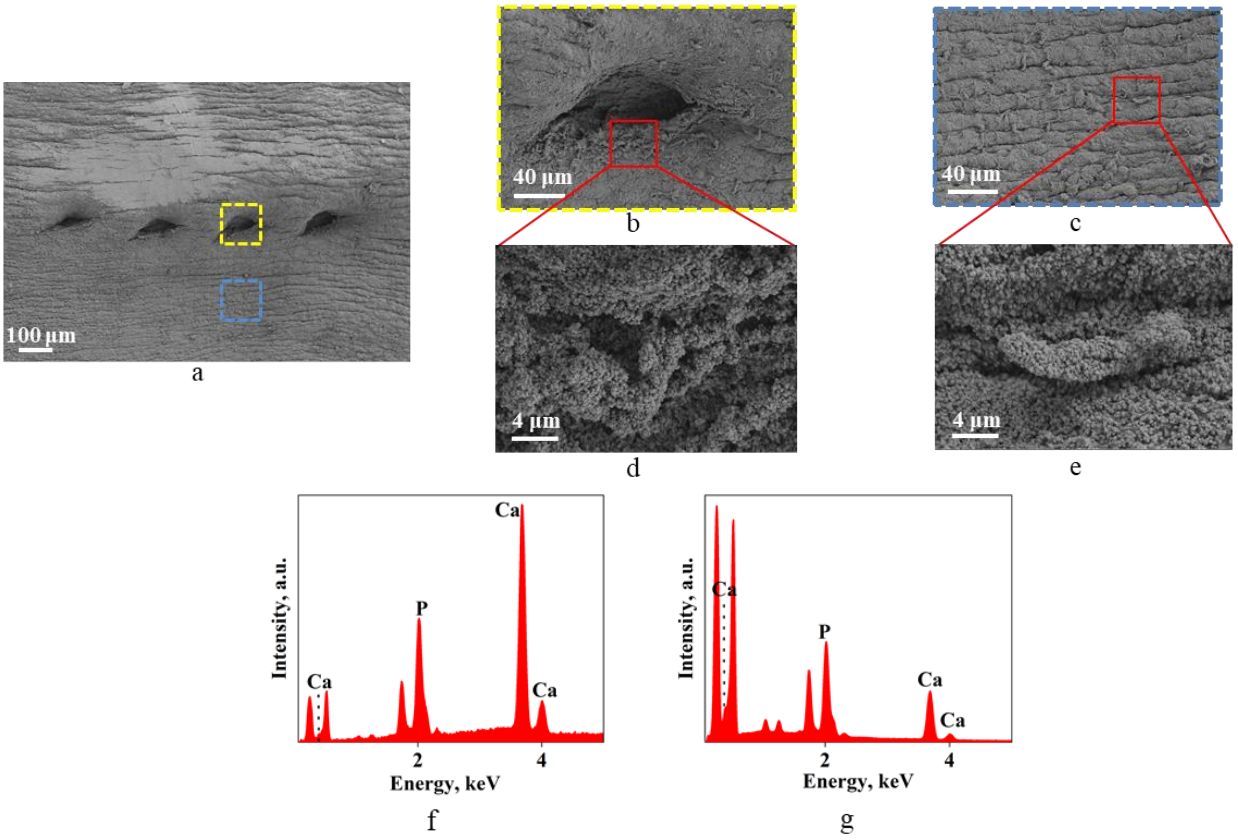

Fig. 5. SEM images and EDS energy spectra of valves in SBF with 5 days of calcification: a – overall surface morphology; b, c, d, e – enlarged image of the corresponding area; f, g – corresponding EDS energy spectrum

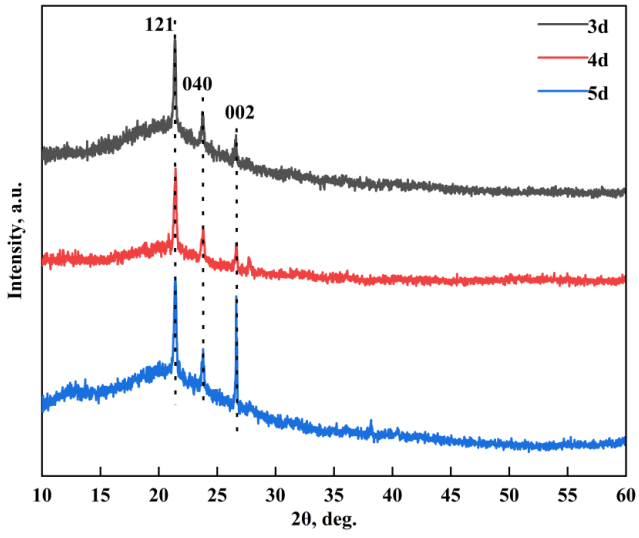

Fig. 6. XRD pattern of valves with different days of calcification

The FTIR-ATR spectra of the control (CAV) and experimental (EAV) valves measured are shown in Fig. 7. The weak band at 520 cm^{-1} in the range of 2000 – 500 cm^{-1} may be from HAp. The presence of weak splitting peaks at 560 cm^{-1} and 600 cm^{-1} follows the characteristic peaks of PO_4^{3-} in apatite [28]. The characteristic absorption peak of the calcium phosphate P-O bond appears at 1026 cm^{-1} [27]. A weak characteristic peak of CO_3^{2-} vibration was shown at 1450 cm^{-1} [27]. Peaks at 1640 cm^{-1} and 1540 cm^{-1} correspond to amide I and II bonds in organic valve components [29]. The FTIR-ATR data confirmed the presence of CO_3^{2-} in the deposits on the valve surface into the interior of the apatite crystals replacing some of the phosphate groups.

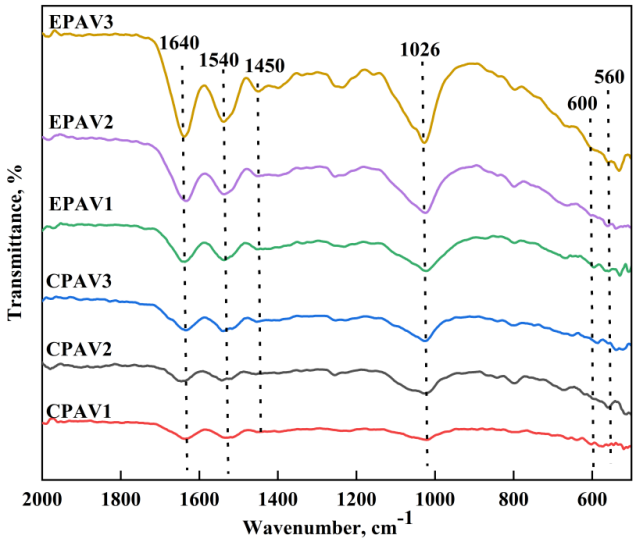

Fig. 7. FTIR-ATR pattern of valves with different days of calcification

TGA was used to quantify calcium deposition differences between CAV and EAV samples (Fig. 8 a). The TGA curves show two main weight loss stages. The first stage (0 – 220 °C) involves water loss from the valve tissue

and partial decomposition of organic matter as DCPD converts to calcium diphosphate [30, 31]; the second stage (240 – 630 °C) shows the highest weight loss, corresponding to the decomposition of extracellular matrix components like collagen, elastin, and glycosaminoglycans, as well as further DCPD decomposition to calcium pyrophosphate; At temperatures greater than 630 °C, the remaining material in the crucible was calcium deposits with higher decomposition temperatures [32, 33]. The percentage of calcium deposits remaining in each sample after 630 °C was obtained from the analysis of TGA data as follows: CAV1 1.9 %, CAV2 2.4 %, CAV3 3.5 %; EAV1 13 %, EAV2 17%, EAV3 20%. From the DTG curves in Fig. 8 b, it can be obtained that the onset temperature of thermal decomposition and the temperature of the maximum weight loss rate were approximately the same for the six samples. The first peak was sharper compared to the second peak, indicating a faster rate of initial water loss and a slower rate of organic matter decomposition.

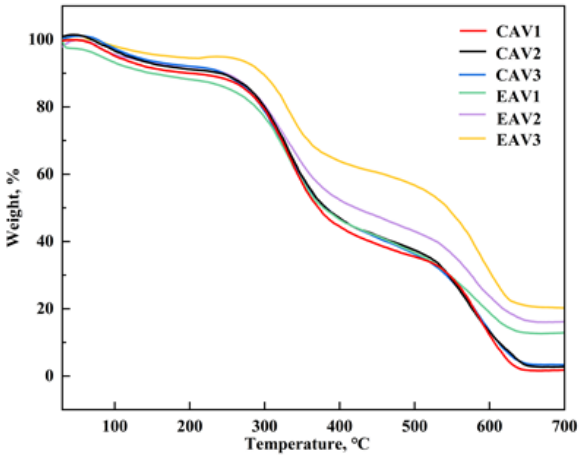

a

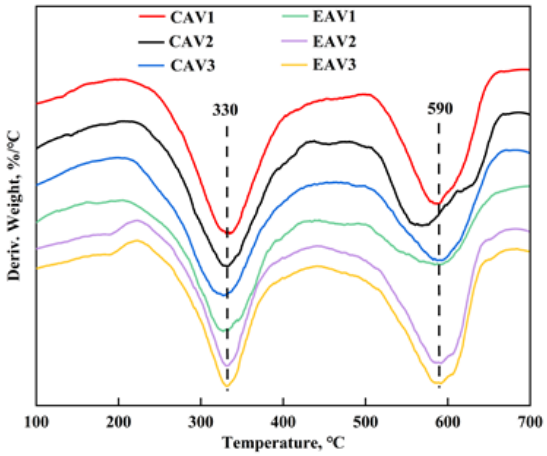

b

Fig. 8. Patterns of valves with different days of calcification: a – TGA; b – DTG

It can be found from the data that CAV and EAV have significantly more calcium deposits than CAV under the same number of days of immersion, and the difference in the calcium deposit content of CAV is not very obvious under the same conditions, whereas the content in EAV can be seen as a significant difference in the diagram. It proves that under the simulated conditions of microneedle microinjury of the valve, microinjury on the valve surface can accelerate the capture of calcium ions in SBF and their surface nucleation and growth.

4. CONCLUSIONS

The study investigated the potential role of microinjuries in promoting calcification of heart valves. Microneedles were used to simulate microinjuries on porcine aortic valves, which were then placed in SBF. The results showed that the microneedle-injured valve areas exhibited a greater tendency to capture calcium from the SBF solution compared to the native valve surfaces. This enhanced calcium capture, facilitating calcium nucleation and subsequent growth near the injured area, potentially due to damaged collagen and altered surface morphology. XRD analysis revealed that the main crystalline phase of the calcium deposits was initially DCPD, which then gradually transformed into the HAp phase over time. These results indicated that microinjuries on the valve surface could accelerate the capture of calcium ions from the surrounding fluid and promote the nucleation and growth of calcium deposits, potentially contributing to calcific aortic valve disease progression. Furthermore, accidental injury, bacterial infection, or hypertension may cause valve damage, and there is also the phenomenon of valve breakage calcification in the clinic, but there is still an absence of simulated valve defect calcification ex vivo. In this study, microneedle-based construction of defective valves was used to mimic the simulation of the early phenomenon of valve calcification, further providing a mimetic model for initiating the calcification of injured valves.

Acknowledgments

This work has been supported by the National Natural Science Foundation of China (No. 51902289).

REFERENCES

1. **Teo, K.K., Corsi, D.J., Tam, J.W., Dumesnil, J.G., Chan, K.L.** Lipid Lowering on Progression of Mild to Moderate Aortic Stenosis: Meta-Analysis of the Randomized Placebo-Controlled Clinical Trials on 2344 Patients *Canadian Journal of Cardiology* 27 (6) 2011: pp. 800 – 808. https://doi.org/10.1016/j.cjca.2011.03.012
2. **Hu, K., Liu, D., Huegel, E., Kreipl, M., Sokalski, V., Lau, K., Lengenfelder, B., Ertl, G., Frantz, S., Nordbeck, P.** Impact of Single-Valve and Multiple-Valve Heart Disease on Long-Term Outcome in Patients with Chronic Heart Failure *European Heart Journal* 44 (2) 2023: pp. ehad655.1624. https://doi.org/10.1093/eurheartj/ehad655.1624
3. **Tong, Q., Cai, J., Wang, Z., Sun, Y., Liang, X., Xu, Q., Mahamoud, O.A., Qian, Y., Qian, Z.** Recent Advances in the Modification and Improvement of Bioprosthetic Heart Valves 20 (23) *Small* 2024: pp. 2309844. https://doi.org/10.1002/smll.202309844
4. **Li, C., Xu, S., Gotlieb, A.I.** The Response to Valve Injury. A Paradigm to Understand the Pathogenesis of Heart Valve Disease *Cardiovascular Pathology* 20 (3) 2011: pp. 183 – 190. https://doi.org/10.1016/j.carpath.2010.09.008

5. **Akat, K., Borggrefe, M., Kaden, J.J.** Aortic Valve Calcification: Basic Science to Clinical Practice *Heart* 95 (8) 2009: pp. 616 – 623. https://doi.org/10.1136/hrt.2007.134783
6. **Gourgas, O., Khan, K., Schwertani, A., Cerruti, M.** Differences in Mineral Composition and Morphology Between Men and Women in Aortic Valve Calcification *Acta Biomaterialia* 106 2020: pp. 342 – 350. https://doi.org/10.1016/j.actbio.2020.02.030
7. **Aggarwal, S.R., Clavel, M.A., Messika-Zeitoun, D., Cueff, C., Malouf, J., Araoz, P.A., Mankad, R., Michelena, H., Vahanian, A., Enriquez-Sarano, M.** Sex Differences in Aortic Valve Calcification Measured by Multidetector Computed Tomography in Aortic Stenosis *Circulation: Cardiovascular Imaging* 6 (1) 2013: pp. 40 – 47. https://doi.org/10.1161/CIRCIMAGING.112.980052
8. **Rawshani, A., Sattar, N., McGuire, D.K., Wallström, O., Smith, U., Borén, J., Bergström, G., Omerovic, E., Rosengren, A., Eliasson, B., Bhatt, D.L., Rawshani, A.** Left-Sided Degenerative Valvular Heart Disease in Type 1 and Type 2 Diabetes *Circulation* 146 (5) 2022: pp. 398 – 411. https://doi.org/10.1161/CIRCULATIONAHA.121.058072
9. **Lu, Q., Lv, J., Ye, Y., Li, Z., Wang, W., Zhang, B., Zhao, Q., Zhao, Z., Zhang, H., Liu, Q., Wang, B., Yu, Z., Guo, S., Duan, Z., Zhao, Y., Gao, R., Xu, H., Wu, Y.** Prevalence and Impact of Diabetes in Patients with Valvular Heart Disease *iScience* 27 (3) 2024: pp. 109084. https://doi.org/10.1016/j.isci.2024.109084
10. **Lindman, B.R., Clavel, M.A., Mathieu, P., Iung, B., Lancellotti, P., Otto, C.M., Pibarot, P.** Calcific Aortic Stenosis *Nature Reviews Disease Primers* 2 (1) 2016: pp. 16006. https://doi.org/10.1038/nrdp.2016.6
11. **Aviv, Y., Nassar, M., Perlman, G., Arow, Z., Lessick, J., Danenberg, H., Vaknin-Assa, H., Finkelstein, A., Kornowski, R., Hamdan, A.** Differences in Valve Morphology Between Patients with Bicuspid and Tricuspid Aortic Valve *European Heart Journal* 41 (2) 2020: pp. ehaa946.0166. https://doi.org/10.1093/ehjci/ehaa946.0166
12. **Pierlot, C.M., Moeller, A.D., Lee, J.M., Wells, S.M.** Pregnancy-Induced Remodeling of Heart Valves *American Journal of Physiology-Heart and Circulatory Physiology* 309 (9) 2015: pp. H1565 – H1578. https://doi.org/10.1152/ajpheart.00816.2014
13. **Pierlot, C.M., Lee, J.M., Amini, R., Sacks, M.S., Wells, S.M.** Pregnancy-Induced Remodeling of Collagen Architecture and Content in the Mitral Valve *Annals of Biomedical Engineering* 42 (10) 2014: pp. 2058 – 2071. https://doi.org/10.1007/s10439-014-1077-6
14. **Taylor, P.M.** Biological Matrices and Bionanotechnology *Philosophical Transactions of the Royal Society B: Biological Sciences* 362 (1484) 2007: pp. 1313 – 1320. https://doi.org/10.1098/rstb.2007.2117
15. **Patel, A., Fine, B., Sandig, M., Mequanint, K.** Elastin Biosynthesis: The Missing Link in Tissue-Engineered Blood Vessels *Cardiovascular Research* 71 (1) 2006: pp. 40 – 49. https://doi.org/10.1016/j.cardiores.2006.02.021
16. **Johnson, N.A., Sengupta, S., Saidi, S.A., Lessan, K., Charnock-Jones, S.D., Scott, L., Stephens, R., Freeman, T.C., Tom, B.D.M., Harris, M., Denyer, G., Sundaram, M., Sasisekharan, R., Smith, S.K., Print, C.G.** Endothelial Cells Preparing to Die by Apoptosis Initiate a Program of Transcriptome and Glycome Regulation *The FASEB Journal* 18 (1) 2004: pp. 188 – 190. https://doi.org/10.1096/fj.03-0097fje
17. **Moncla, L.H.M., Briend, M., Bossé, Y., Mathieu, P.** Calcific Aortic Valve Disease: Mechanisms, Prevention and Treatment *Nature Reviews Cardiology* 20 (8) 2023: pp. 546 – 559. https://doi.org/10.1038/s41569-023-00845-7
18. **Kodigepalli, K.M., Thatcher, K., West, T., Howsmon, D.P., Schoen, F.J., Sacks, M.S., Breuer, C.K., Lincoln, J.** Biology and Biomechanics of the Heart Valve Extracellular Matrix *Journal of Cardiovascular Development and Disease* 7 (4) 2020: pp. 57. https://doi.org/10.3390/jcdd7040057
19. **Jansen, F., Xiang, X., Werner, N.** Role and Function of Extracellular Vesicles in Calcific Aortic Valve Disease *European Heart Journal* 38 (36) 2017: pp. 2714 – 2716. https://doi.org/10.1093/eurheartj/ehx477
20. **Zheng, K.H., Tsimikas, S., Pawade, T., Kroon, J., Jenkins, W.S.A., Doris, M.K., White, A.C., Timmers, N.K.L.M., Hjortnaes, J., Rogers, M.A., Aikawa, E., Arsenault, B.J., Witztum, J.L., Newby, D.E., Koschinsky, M.L., Fayad, Z.A., Stroes, E.S.G., Boekholdt, S.M., Dweck, M.R.** Lipoprotein(a) and Oxidized Phospholipids Promote Valve Calcification in Patients With Aortic Stenosis *Journal of the American College of Cardiology* 73 (17) 2019: pp. 2150 – 2162. https://doi.org/10.1016/j.jacc.2019.01.070
21. **Kostyunin, A.E., Yuzhalin, A.E., Ovcharenko, E.A., Kutikhin, A.G.** Development of Calcific Aortic Valve Disease: Do We Know Enough for New Clinical Trials? *Journal of Molecular and Cellular Cardiology* 132 2019: pp. 189 – 209. https://doi.org/10.1016/j.yjmcc.2019.05.016
22. **Niu, L., Jee, S.E., Jiao, K., Tonggu, L., Li, M., Wang, L., Yang, Y., Bian, J., Breschi, L., Jang, S.S., Chen, J., Pashley-David, H., Tay-Franklin, R.** Collagen Intrafibrillar Mineralization as a Result of the Balance Between Osmotic Equilibrium and Electroneutrality *Nature Materials* 16 (3) 2017: pp. 370 – 378. https://doi.org/10.1038/nmat4789
23. **Kim, D., Lee, B., Thomopoulos, S., Jun, Y.S.** In Situ Evaluation of Calcium Phosphate Nucleation Kinetics and Pathways during Intra- and Extrafibrillar Mineralization of Collagen Matrices *Crystal Growth & Design* 16 (9) 2016: pp. 5359 – 5366. https://doi.org/10.1021/acs.cgd.6b00864
24. **Xue, Z., Yang, M., Xu, D.** Nucleation of Biomimetic Hydroxyapatite Nanoparticles on the Surface of Type I Collagen: Molecular Dynamics Investigations *The Journal of Physical Chemistry C* 123 (4) 2019: pp. 2533 – 2543. https://doi.org/10.1021/acs.jpcc.8b10342
25. **Qin, D., Xue, Z., Du, M., Wang, X., Xue, Y., Xu, D.** Molecular Dynamics Exploration of Ion Association Mechanism of Apatite Controlled by a Nanogrooved Hydroxyapatite Surface *Applied Surface Science* 617 2023: pp. 156580. https://doi.org/10.1016/j.apsusc.2023.156580
26. **Lou, X., Vijayasekaran, S., Sugiharti, R., Robertson, T.** Morphological and Topographic Effects on Calcification Tendency of pHEMA Hydrogels *Biomaterials* 26 (29) 2005: pp. 5808 – 5817. https://doi.org/10.1016/j.biomaterials.2005.02.034
27. **Kuranov, G., Nikolaev, A., Frank-Kamenetskaya, O., Gulyaev, N., Volina, O.** Physicochemical Characterization of

Human Cardiovascular Deposits *JBIC Journal of Biological Inorganic Chemistry* 24 (7) 2019: pp. 1047 – 1055. https://doi.org/10.1007/s00775-019-01714-w

28. **Niu, X., Chen, S., Tian, F., Wang, L., Feng, Q., Fan, Y.** Hydrolytic Conversion of Amorphous Calcium Phosphate into Apatite Accompanied by Sustained Calcium and Orthophosphate Ions Release *Materials Science and Engineering: C* 70 2017: pp. 1120 – 1124. https://doi.org/10.1016/j.msec.2016.04.095
29. **Delogne, C., Lawford, P.V., Habesch, S.M., Carolan, V.A.** Characterization of the Calcification of Cardiac Valve Bioprostheses by Environmental Scanning Electron Microscopy and Vibrational Spectroscopy *Journal of Microscopy* 228 (1) 2007: pp. 62 – 77. https://doi.org/10.1111/j.1365-2818.2007.01824.x
30. **Dabiri, S.M.H., Lagazzo, A., Barberis, F., Farokhi, M., Finochio, E., Pastorino, L.** Characterization of Alginate-brushite In-situ Hydrogel Composites *Materials Science and Engineering: C* 67 2016: pp. 502 – 510. https://doi.org/10.1016/j.msec.2016.04.104
31. **Bamzai, K.K., Suri, S., Singh, V.** Synthesis, Characterization, Thermal and Dielectric Properties of Pure and Cadmium Doped Calcium Hydrogen Phosphate *Materials Chemistry and Physics* 135 (1) 2012: pp. 158 – 167. https://doi.org/10.1016/j.matchemphys.2012.04.040
32. **Mansour, S.F., El-dek, S.I., Ahmed, M.A., Abd-Elwahab, S.M., Ahmed, M.K.** Effect of Preparation Conditions on the Nanostructure of Hydroxyapatite and Brushite Phases *Applied Nanoscience* 6 (7) 2016: pp. 991 – 1000. https://doi.org/10.1007/s13204-015-0509-4
33. **Madhurambal, G., Subha, R., Mojumdar, S.C.** Crystallization and Thermal Characterization of Calcium Hydrogen Phosphate Dihydrate Crystals *Journal of Thermal Analysis and Calorimetry* 96 (1) 2009: pp. 73 – 76. https://doi.org/10.1007/s10973-008-9841-1